Inorganic Chemistry

Article

pubs.acs.org/IC

Multifunctional SiO_2@Gd_2O_3:Yb/Tm Hollow Capsules: Controllable Synthesis and Drug Release Properties

Guixin Yang, Ruichan Lv, Shili Gai, Yunlu Dai, Fei He, and Piaoping Yang*

Key Laboratory of Superlight Materials and Surface Technology, Ministry of Education, College of Material Sciences and Chemical Engineering, Harbin Engineering University, Harbin 150001, P. R. China

ABSTRACT: A series of hollow and luminescent capsules have been fabricated by covering luminescent Gd_2O_3:Yb/Tm nanoparticles on the surface of uniform hollow mesoporous silica capsules (HMSCs), which were obtained from an etching process using Fe_3O_4 as hard templates. X-ray diffraction (XRD), scanning electron microscopy (SEM), transmission electron microscopy (TEM), high-resolution transmission electron microscopy (HRTEM), up-conversion (UC) fluorescence spectra, and N_2 adsorption−desorption were used to characterize these samples. It is found that the as-prepared products have mesoporous pores, large specific surface, and high dispersity. In particular, the size, shape, surface area, and interior space of the composites can be finely tuned by adjusting the size and morphology of the magnetic cores. Under 980 nm near-infrared (NIR) laser irradiation, the composites show characteristic blue UC emissions of Tm^{3+} even after carrying doxorubicin hydrochloride (DOX). The drug-release test reveals that the capsules showed an apparent sustained release character and released in a pH-sensitive manner. Interestingly, the UC luminescence intensity of the drug-carrying system increases with the released DOX, realizing the possibility to track or monitor the released drug by the change of UC fluorescence simultaneously, which should be highly promising in anticancer drug delivery and targeted cancer therapy.

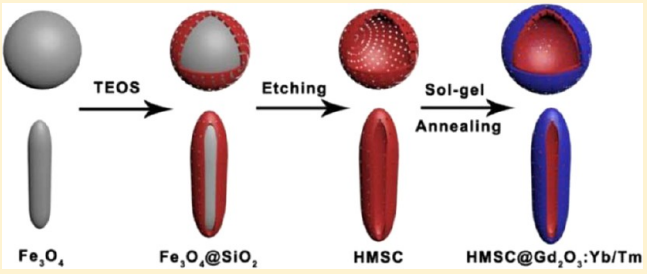

INTRODUCTION

Recently, many efforts have been devoted to the preparation and exploitation of novel sustained drug systems owing to their high transportation efficiency, low side reaction, and low toxicity.[1−8] So far, diverse polymer,[9−11] inorganic,[12−15] and organic/inorganic hybrid materials[16−18] with various structures have been extensively used as carriers for drug release. Among them, mesoporous silica-based materials[19,20] have attracted special interest for biological applications owing to their high biodegradability, biocompatibility, controllable mesoporous structure, high specific surface area, and easy surface decoration.[21−24] In particular, embedded, core−shell, and rattle-type structured materials are of special interest due to the results of combining functional moieties including magnetic nanoparticles,[25−28] Au nanoparticles,[29] quantum dots,[30−32] tumor-targeting groups,[33−35] and polyethylene glycol (PEG)[36−39] with the surface of mesoporous silica. Multifunctional silica-based materials have obvious advantages such as drug delivery, bioimaging diagnosis, and cancer therapy.[37] However, in most cases, the degree of functional covering is low and the coating is not uniform. Meanwhile, compared with the conventional solid structure, hollow structures are advantaged because they simultaneously have mesoporous shells, a large cavity, and a large surface area. The large cavity and large surface area can store/adsorb more drug molecules than the solid ones, and the mesoporous shells could afford accessible channels for mass transfer and drug diffusion. Meanwhile, they can control the penetrability of the shell for matter exchange between the outer environment and the inner voids. Therefore, hollow structures in the drug delivery systems can easily be monitored and identified to assess the drug release and disease therapy efficiency. Thus, developing a novel series of multifunctional hollow structured mesoporous silica capsules should be of great prospect, not only because of their silica properties but due to their large cavity and controllable mesoporous shell, which is feasible for loading more drug molecules and making the drug molecules freely diffuse the mesopores.

In general, fluorescence-functionalized mesoporous silica as drug-carrying vehicles were prepared by grafting luminescent materials onto mesoporous silica.[38] In comparison with organic dyes and quantum dots (QDs), rare earth-based materials have obvious virtues, including avoiding the photobleaching[39] and chronic toxicities[40] because of their high chemical stability and intrinsic low phonon energies, and therefore should be suitable candidates in biomedical applications. To date, great effort has been devoted to the development of various routes for rare earth-doped materials for drug release[41−43] and core−shell structured multifunctional materials.[44−48] Furthermore, unlike the wide studies on magnetic particle-modified silica used as drug carriers, luminescence, especially rare earth-based UC phosphor-functionalized hollow silica particles, has been relatively less researched. It is well accepted that the potential probability of the UC emissions irradiated by the NIR laser may be a facile, effective, and real-time method to track the drug-delivery route in a living system. Thus, it is highly desirable to

Received: May 17, 2014
Published: October 6, 2014

   dx.doi.org/10.1021/ic501121t | *Inorg. Chem.* 2014, 53, 10917−10927

Scheme 1. Schematic Illustration of the Synthetic Procedure for HMSC@Gd_2O_3:Yb/Tm Composite

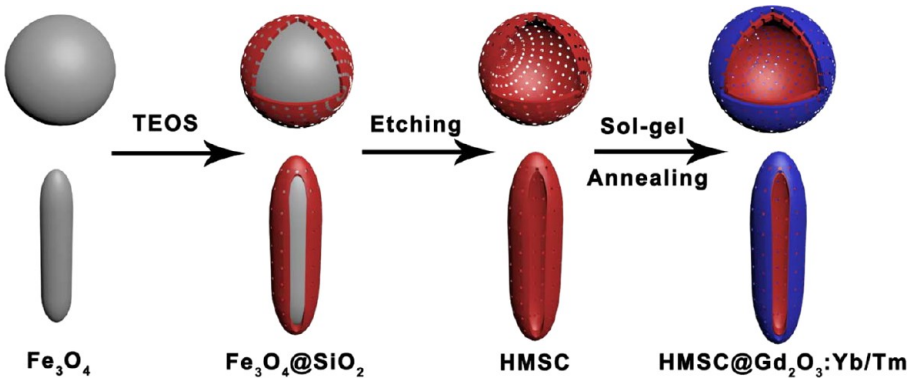

design a novel kind of functional hollow mesoporous silica capsules, which simultaneously have hollow and mesoporous structure and UC fluorescent property.

Nowadays, diverse routes have been employed to produce HMSCs such as self-assembly,[49] coprecipitation, surface reaction,[50] sol–gel process,[51] metal-organic chemical vapor deposition (MOCVD),[52] etc. Most HMSCs were prepared by template methods including preparation of inner cores and outer shells, followed by the subsequent removal of the core material. Magnetic particles with easily adjusted particle shape and size have been widely used as core materials. An alternative etching procedure to eliminate the magnetic cores of as-fabricated Fe_3O_4@SiO_2 is an efficient route to produce hollow silica particles.[53,54] Currently, rare earth-based materials have been extensively used as fluorescent components for versatile applications owing to their unique physiochemical characteristics arising from the 4f electronic shells.[55−63] As one of the efficient matrix materials for green and blue UC emissions when doping Yb^{3+}/Er^{3+} and Yb^{3+}/Tm^{3+}, Gd_2O_3:Ln has gained much attention in biomedical fields.[64−67]

Here in this work, we proposed a facile procedure to prepare Gd_2O_3:Yb/Tm coated hollow mesoporous silica capsules (denoted as HMSC@Gd_2O_3:Yb/Tm) with large surface areas and hollow structures employing Fe_3O_4 nanoparticles as a sacrificial template. The size and morphology of the Fe_3O_4 cores were changed to alter the shape and textural features of the final hollow capsules. It is noted that, in comparison with other well-developed synthetic processes to prepare hollow materials, this procedure is much more effective, facile, and scalable. Drug-release properties were tested by using DOX as a model drug. Moreover, 3-(4,5-dimethylthiazol-2-yl)-2,5-diphenyltetrazolium bromide (MTT) cytotoxicity assays were also tested for potential biomedical application.

EXPERIMENTAL SECTION

Materials. $FeCl_3·6H_2O$, ethylene glycol (EG), diethylene glycol (DEG), sodium acetate (CH_3COONa), sodium acrylate, ammonia (25–28%), tetraethoxysilane (TEOS), cetyltrimethylammonium bromide (CTAB), polyethylene glycol (PEG, mol wt = 10 000 g mol^{-1}), hydrochloric acid (A. R.), Gd_2O_3 (99.99%), Tm_2O_3 (99.99%), and Yb_2O_3 (99.99%) were all from Sinopharm Chemical Reagent Co., Ltd. (China). DOX is obtained from Nanjing Duodian Chemical Limited Company. $Gd(NO_3)_3$, $Yb(NO_3)_3$, and $Tm(NO_3)_3$ were fabricated by dissolving Gd_2O_3, Yb_2O_3, and Tm_2O_3 in dilute nitric acid, followed by the evaporation of the superfluous acid and water.

Synthesis of Fe_3O_4 Particles with Tunable Size and Shape. Fe_3O_4 spheres with an average size of 100 nm were synthesized by the method in the literature with some modification.[68] Typically, 0.54 g of $FeCl_3·6H_2O$, 1.5 g of Na acrylate, and 1.5 g of CH_3COONa were dissolved in a mixed solvent containing 12 mL of DEG and 8 mL of EG with stirring. After stirring for 30 min, the as-obtained solution was transferred into a Teflon-lined autoclave and kept at 200 °C for 10 h. After naturally cooling to room temperature, the as-prepared product was rinsed with deionized water and ethanol several times and then dried in vacuum for 12 h to gain the final product, which was denoted as Fe_3O_4-A. Fe_3O_4 spheres with a mean size of 180 nm were prepared by a similar process except that the mixed solvent (DEG/EG) was replaced by 20 mL of EG by keeping other conditions unchanged. The obtained product was designated as Fe_3O_4-B. Fe_3O_4 spheres with the particle size of 220 and 290 nm were prepared by changing the sodium acrylate/sodium acetate weight ratio of 1.5/0, 1.5/0.5, respectively. The respective products were denoted Fe_3O_4-C and Fe_3O_4-D.

Rod-like iron-based particles were prepared by the following procedure. Briefly, 1.08 g of $FeCl_3·6H_2O$ and 0.9 g of polyvinylpyrrolidone (PVP) were dissolved in 60 mL of deionized water under stirring; the solution was then transferred to a 100 mL Teflon-lined autoclave and heated at 100 °C for 10 h. Then the particles were gathered by centrifugation, washed with water and ethanol three times, and dried in vacuum at room temperature for 24 h.

Preparation of Hollow Mesoporous SiO_2 Capsules (HMSC). First, core–shell structured Fe_3O_4@SiO_2 particles were prepared by a modified Stöber sol–gel route. Typically, Fe_3O_4 particles (100 mg) with a mean particle size of 90 nm were ultrasonically treated with 0.1 mol L^{-1} HCl for 0.5 h. Subsequently, the sample was added into a solution including ethanol (80 mL), CTAB (0.1 g), ammonia (1 mL), and deionized water (20 mL). Then 0.07 mL of TEOS was added dropwise to the solution with stirring for 12 h at room temperature to obtain Fe_3O_4@SiO_2. Second, core–shell structured Fe_3O_4@SiO_2 particles were treated with HCl (37%) at 60 °C and then separated by centrifugation. The acquired product was dried in vacuum at 60 °C for 24 h and was designated as HMSC-A. HMSC-B, HMSC-C, HMSC-D, and HMSC-E with different sizes and shapes were synthesized by a similar procedure.

For comparison, the solid silica with a particle size of ∼220 nm was prepared by a typical Stöber process with some modification.[69] Typically, 31.4 mL of deionized H_2O, 14 mL of TEOS, and 183 mL of NH_4OH were added into 120 mL of ethanol and stirred for 4 h. The solid silica was centrifugally separated from the suspension and washed several times with ethanol.

Synthesis of HMSC@Gd_2O_3:Yb/Tm Composites. $Gd(NO_3)_3$ (0.19 mmol), 0.009 mmol of $Yb(NO_3)_3$, and 0.001 mmol of $Tm(NO_3)_3$ were added to 200 mL of ethanol until dissolution. Then 200 mg of silica capsules was introduced to the solution under stirring. After ultrasonication at 70 °C for 6 h, the as-prepared product was dried at 60 °C for 6 h and then kept at 700 °C for 5 h. The final products were designed as HMSC-A@Gd_2O_3:Yb/Tm, HMSC-B@Gd_2O_3:Yb/Tm, HMSC-C@Gd_2O_3:Yb/Tm, HMSC-D@Gd_2O_3:Yb/Tm, HMSC-E@Gd_2O_3:Yb/Tm.

DOX Release Test. DOX was selected as a model drug to study the drug loading and release properties as a common anticancer drug. In a typical procedure for the carrying of DOX on HMSC@Gd_2O_3:Yb/Tm, 30 mg of HMSC@Gd_2O_3:Yb/Tm nanocapsules were

dx.doi.org/10.1021/ic501121t | Inorg. Chem. 2014, 53, 10917−10927

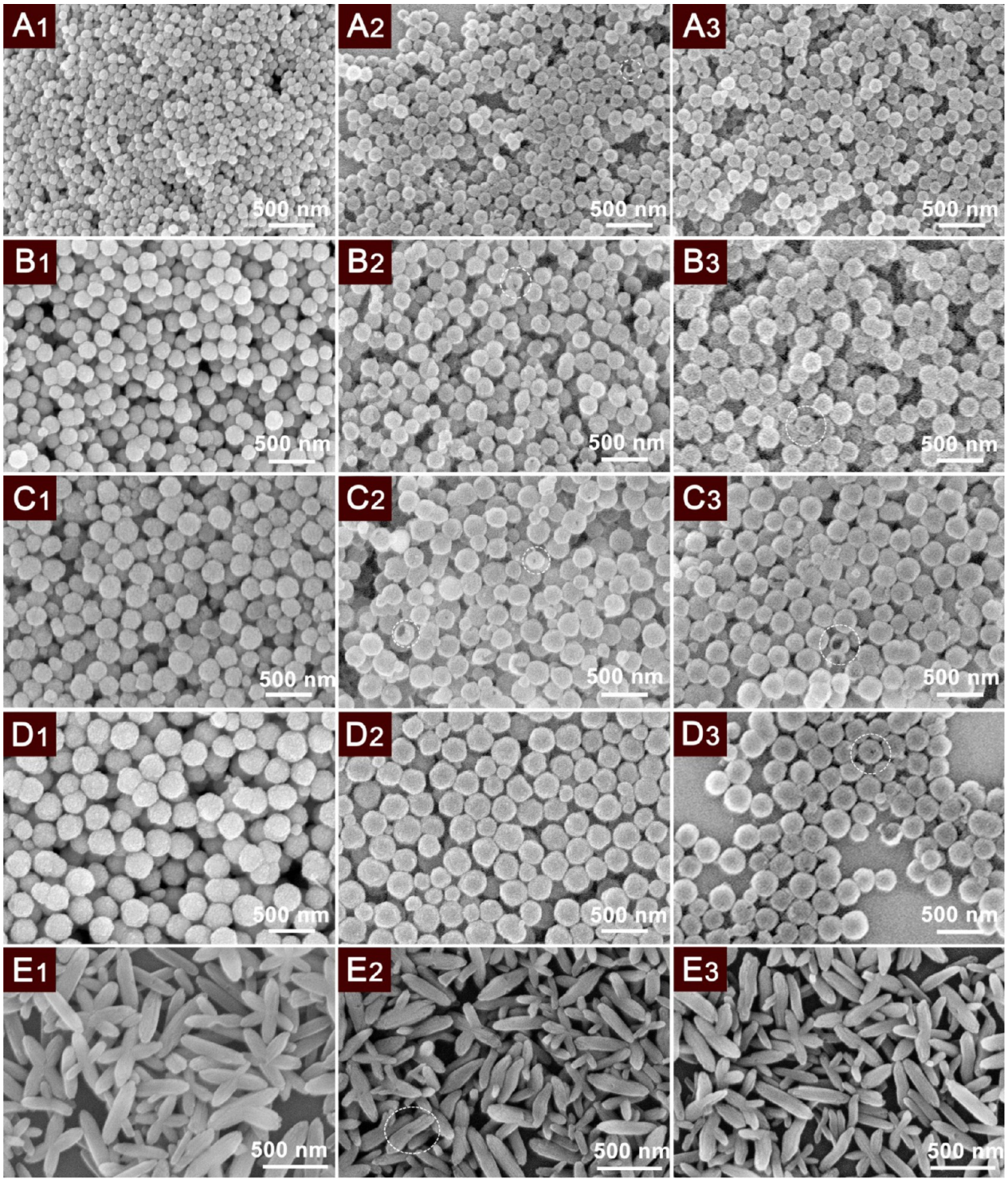

Figure 1. SEM images of Fe_3O_4-A (A1), HMSC-A (A2), HMSC-A@Gd_2O_3:Yb/Tm (A3); Fe_3O_4-B (B1), HMSC-B (B2), HMSC-B@Gd_2O_3:Yb/Tm (B3); Fe_3O_4-C (C1), HMSC-C (C2), HMSC-C@Gd_2O_3:Yb/Tm (C3); Fe_3O_4-D (D1), HMSC-D (D2), HMSC-D@Gd_2O_3:Yb/Tm (D3); Fe_3O_4-E (E1), HMSC-E (E2), HMSC-E@Gd_2O_3: Yb/Tm (E3).

dispersed in 5 mL of DOX solution (0.5 mg/mL). The sample was protected from light, slightly shaken for 24 h at room temperature, and then washed with the phosphate-buffered saline (PBS) solution, giving rise to the DOX-carried product, which was designated as HMSC-C@Gd_2O_3:Yb/Tm-DOX. The amount of DOX loaded in the products was determined by UV−vis spectra at a wavelength of 480 nm. The loading efficiency (LE%) was measured as follows: LE% = $(M_{DOX1} - M_{DOX2})/M_{DOX1} \times 100\%$, where M_{DOX1} is the initial DOX amount and M_{DOX2} is the unloaded amount of DOX. The release test was carried out by dispersing HMSC@Gd_2O_3:Yb/Tm-DOX in 10 mL of PBS solution under slow stirring under dark conditions, and the temperature was maintained at 37 °C. PBS solution was taken for measurement and quickly replaced by the same amount of fresh PBS at a selected time interval.

Hemolysis Assay. The red blood cells were acquired by eliminating the serum from the EDTA.K2 stabilized human blood through washing with 1% normal saline and centrifugation five times. After that, the blood cells were diluted to 1/10 with PBS solution (pH = 7.4).

dx.doi.org/10.1021/ic501121t | *Inorg. Chem.* 2014, 53, 10917−10927

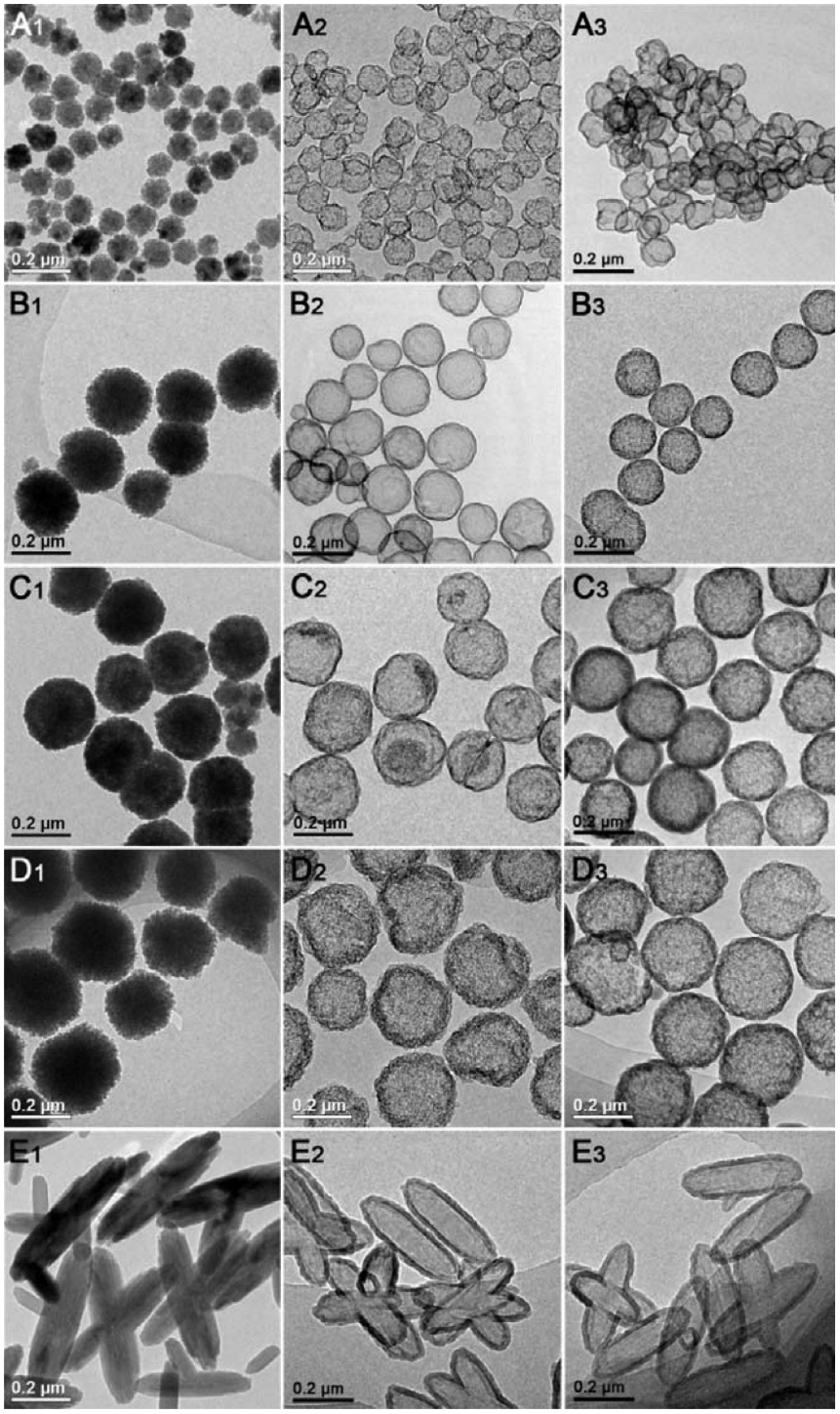

Figure 2. TEM images of Fe_3O_4-A (A1), HMSC-A (A2), HMSC-A@Gd_2O_3:Yb/Tm (A3); Fe_3O_4-B (B1), HMSC-B (B2), HMSC-B@Gd_2O_3:Yb/Tm (B3); Fe_3O_4-C (C1), HMSC-C (C2), HMSC-C@Gd_2O_3:Yb/Tm (C3); Fe_3O_4-D (D1), HMSC-D (D2), HMSC-D@Gd_2O_3:Yb/Tm (D3); Fe_3O_4-E (E1), HMSC-E (E2), HMSC-E@Gd_2O_3:Yb/Tm (E3).

Then the diluted cells suspension (0.4 mL) was mixed with 1.6 mL of PBS as a negative control, 1.6 mL of deionized water as a positive control, and 1.6 mL of the materials suspensions (1.6 mL) with varying concentrations (7.81, 15.63, 31.25, 62.5, 125, 250, 500, and 1000 μg mL^{-1}). The 10 samples were shaken and kept stable for 2 h at room temperature. In the end, the mixture was centrifuged and the upper supernatants were measured by UV−vis spectroscopy. The hemolysis percentage was calculated by the following equation: hemolysis % = $(A_{sample} - A_{control(-)})/(A_{control(+)} - A_{control(-)})$, where A is the absorbance of UV−vis spectra.

Cellular Uptake. Cellular uptake by HeLa tumor cells was examined using flow cytometry and confocal laser scanning microscope (CLSM). In a typical procedure for flow cytometry test, the as-prepared HMSC-C@Gd_2O_3:Yb/Tm was first labeled with fluorescent dye. HMSC-C@Gd_2O_3:Yb/Tm (20 mg) was dispersed into 20 mL of ethanol; a certain amount of fluorescein isothiocyanate (FITC) was then added, and the mixture was stirred in the dark for 12 h. The as-prepared HMSC-C@Gd_2O_3:Yb/Tm-FITC was centrifuged, rinsed with ethanol, and dried under vacuum. HeLa cells were seeded in 6-well culture plates and grown overnight. The cells were then incubated with

dx.doi.org/10.1021/ic501121t | Inorg. Chem. 2014, 53, 10917−10927

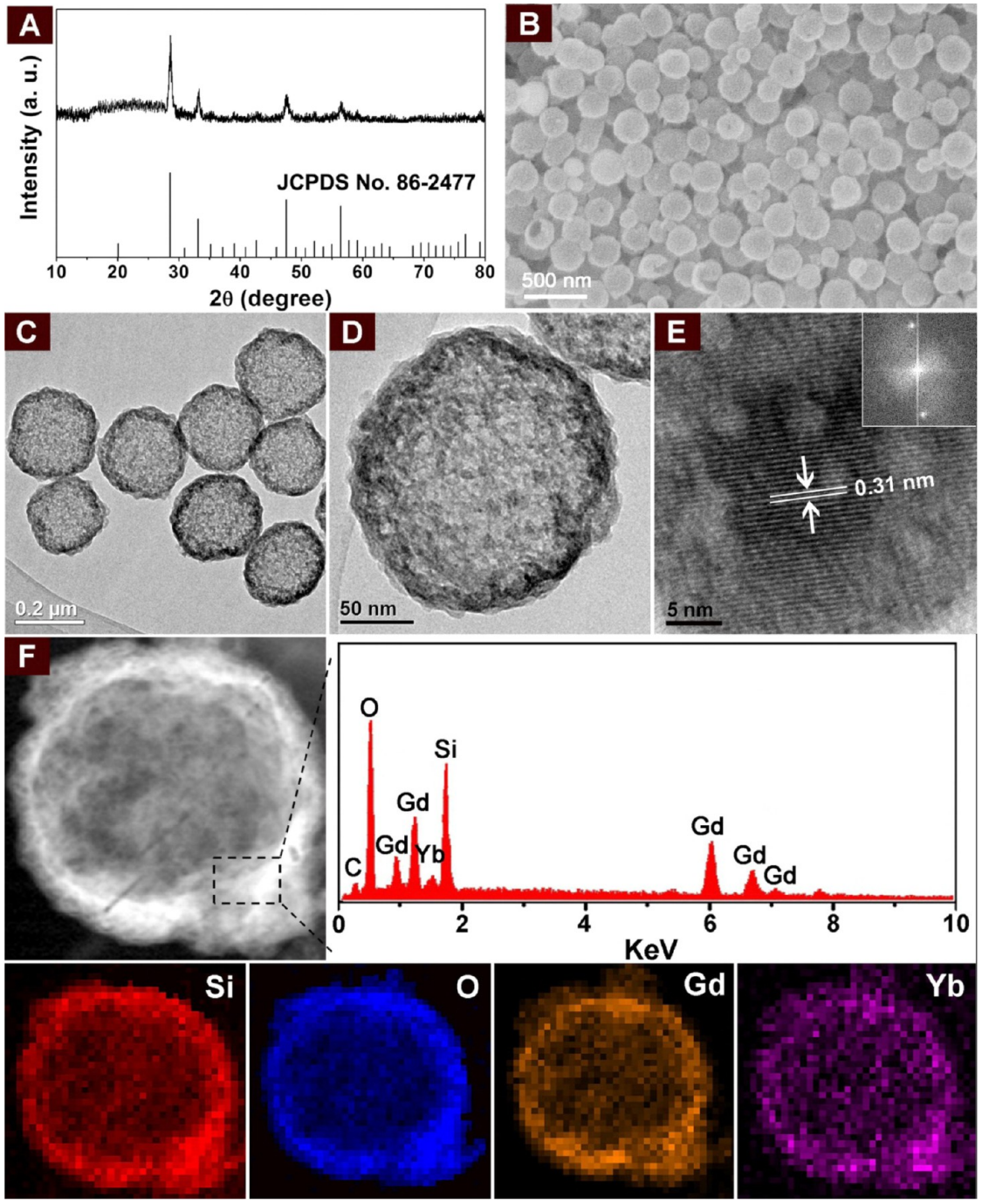

Figure 3. XRD pattern (A), SEM (B), low-magnified TEM (C), high-magnified TEM (D), and HRTEM (E) images; inset in panel E is the corresponding fast Fourier transform (FFT) image. Energy-dispersive spectrometry (EDS) and mapping of HMSC-C@Gd_2O_3:Yb/Tm composite (F).

HMSC-C@Gd_2O_3:Yb/Tm-FITC at 37 °C for 30 min and 3 h, respectively. Through trypsinization, a single cell suspension was obtained and then filtrated through 35 mm nylon mesh. After that, the cells were lifted with a cell stripper and analyzed by a flow cytometer (FACS Calibur). Cells incubated in the absence of the samples were used for control.

Cellular uptake by HeLa tumor cells was measured on a confocal laser scanning microscope (CLSM). The HeLa cells were seeded in a 6-well culture plate, where a clean coverslip was put in each well, and they were grown overnight. After that, the cells were incubated with HMSC@Gd_2O_3:Yb/Tm+DOX for 30 min, 3 h, and 6 h at 37 °C, respectively. Subsequently, the cells were washed with PBS solution three times, fixed with 2.5% formaldehyde (1 mL/well) for 10 min at 37 °C, and then washed with PBS solution three times. To carry out nucleus labeling, the cells were stained with 4′,6-diamidino-2-phenylindole (DAPI) solution (20 μg mL^{-1} in PBS, 1 mL/well) for 10 min and then washed with PBS three times. The samples were measured by CLSM (Leica TCS SP8).

Cytotoxicity of the Samples. The in vitro short-term cytotoxicity of the sample was measured by the standard 3-(4,5-dimethylthiazol-2-yl)-2,5-diphenyltetrazolium bromide (MTT) assay performed on L929 fibroblast cells. In a typical process, L929 cells were plated out with a density of 5000−6000 cells per well in a 96-well plate, leaving 8 wells empty for blank control, then incubated at 37 °C for 24 h in CO_2 (5%) to allow the cells to attach to the wells. The HMSC@Gd_2O_3:Yb/Tm sample was first irradiated by UV light and then diluted with serial concentrations of 7.8125, 15.625, 31.25, 62.5, 125, and 250 μg/mL in the growth media; the cells were incubated constantly using the same

dx.doi.org/10.1021/ic501121t | Inorg. Chem. 2014, 53, 10917−10927

method. Subsequently, MTT (5 mg mL^{-1} in PBS) was introduced and incubated with the cells for an additional 4 h. At last, dimethyl sulfoxide (DMSO) was added to the cell culture at a shaking table. The absorbance spectra of the suspensions were detected by a microplate reader at 570 nm.

Characterization. X-ray diffraction (XRD) spectra were measured on a Rigaku D/max-TTR-III diffractometer using Cu Kα radiation (λ = 0.15405 nm), with a scanning rate of 10°/min in 2θ range from 10° to 80°. Morphological and compositional investigations were performed on a FESEM (Hitachi S-4800), and TEM and HRTEM measurements were performed on a FEI Tecnai G^2 S-Twin transmission electron microscope with a field emission gun operated at 200 kV. Fourier transform IR (FT-IR) spectra were obtained from a PerkinElmer 580B IR spectrophotometer. N_2 sorption measurements were performed at 77 K on a Micromeritics TriStar II 3020. The Brunauer–Emmett–Teller (BET) method was used to determine the specific surface area, and the pore size distribution was obtained by the Barret–Joner–Halenda (BJH) method. UC luminescence was measured by R955 (HAMAMATSU) from 400 to 900 nm using 980 nm LD Module (K98D08M-30W, China) as the excitation source, with an excitation power density of 4 W cm^{-2}. All the measurements were carried out at room temperature.

RESULTS AND DISCUSSION

Phase, Structure, and Shape Evolution. The synthesis procedure of HMSC@Gd_2O_3:Yb/Tm is presented in Scheme 1. A layer of silica is first coated on the as-prepared magnetic particles by a typical Stöber sol–gel process to prepare a core–shell Fe_3O_4@silica structure. Then, the magnetic cores were removed by hydrochloric acid solution, giving rise to the well-dispersed hollow silica capsules with a mesoporous layer. Finally, luminescent Gd_2O_3:Yb/Tm particles were covered on the mesoporous hollow silica capsules to obtain the final bifunctional composite, which was designated as HMSC@Gd_2O_3:Yb/Tm.

A detailed inspection of the as-prepared templates and the resulting products is shown in Figure 1. Well-defined magnetic particles with tunable size and shape were obtained, and the SEM images are displayed in Figure 1A1, B1, C1, D1, and E1. In Figure 1A1–D1, it is obvious that spherical Fe_3O_4 templates are well-dispersed with average diameters of 90, 180, 220, and 300, respectively. From Figure 1E1, we can see that the sample exhibits rod-like morphology with a length of 500 ± 30 nm and a diameter of 180 ± 20 nm. During the etching procedure, the Fe_3O_4 cores could be eliminated from the core–shell structure by hydrochloric acid solution, implying the formation of hollow silica capsules with a large interior space. Using Fe_3O_4 spheres with different size and shape as templates, it is possible to obtain HMSCs with tunable shape and size. In the SEM images of the resulting hollow silica capsules (Figure 1A2, B2, C2, D2, and E2), the size and morphology of the initial Fe_3O_4 templates have mainly been kept. It is noted that the hollow structures of all the HMSCs can be confirmed by the selected broken spheres (pointed by the circles). As for Gd_2O_3:Yb/Tm coated hollow silica capsules (Figure 1A3, B3, C3, D3, and E3), the size and shape can still be maintained, indicating the coating of Gd_2O_3:Yb/Tm layer has little influence on the morphology and size of the final samples. In particular, the cavities in the hollow spheres can yet be found (pointed to by the circles in Figure 1B3, C3, and D3), indicating the existence of the hollow spheres.

The detailed structures of the products were studied in-depth by the TEM images, as shown in Figure 2. It is apparent that well-defined Fe_3O_4 templates with uniform shape and size are acquired (Figure 2A1, B1, C1, and D1), matching well with the SEM results. In addition, the rod-like morphology of Fe_3O_4-E

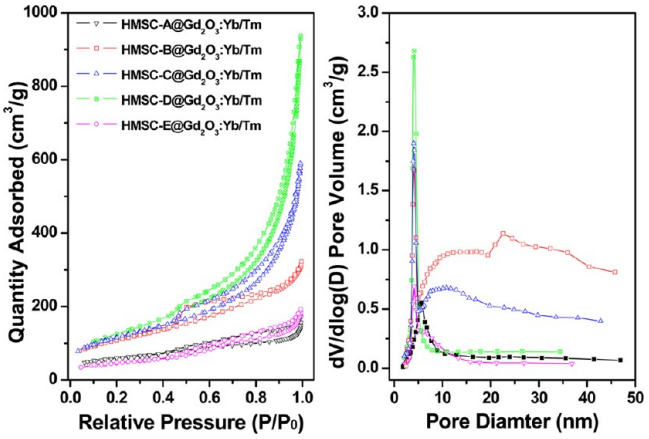

Figure 4. N_2 adsorption/desorption isotherm (left) and pore size distribution (right) of HMSC@ Gd_2O_3:Yb/Tm composites.

Table 1. Specific Surface Area, Average Pore Diameter, And Total Pore Volume of HMSC@Gd_2O_3:Yb/Tm Composites

samples	S_{BET}[a] (m^2/g)	D (nm)	V_P (cm^3/g)
HMSC-A@Gd_2O_3:Yb/Tm	160	7.41	0.31
HMSC-B@Gd_2O_3:Yb/Tm	382	5.58	0.52
HMSC-C@Gd_2O_3:Yb/Tm	461	12.13	1.51
HMSC-D@Gd_2O_3:Yb/Tm	416	9.21	0.95
HMSC-E@Gd_2O_3:Yb/Tm	201	6.42	0.26

[a] S_{BET}, the BET specific surface areas calculated in the relative pressures ranging from 0.05 to 0.2; D, the average diameters of mesopores calculated by the BJH method; V_p, the total pore volumes calculated at the relative pressure of ~0.95.

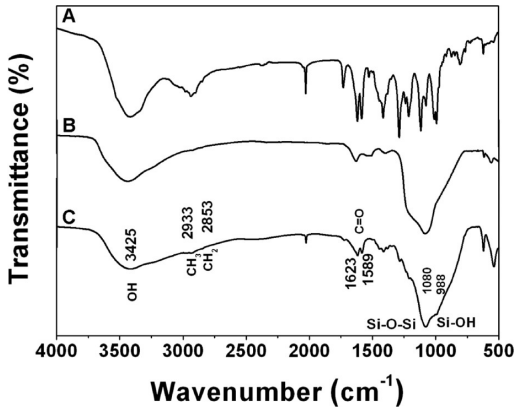

Figure 5. FT-IR spectra of pure DOX (A), HMSC-C@Gd_2O_3:Yb/Tm (B), and HMSC-C@ Gd_2O_3:Yb/Tm-DOX (C).

can also be given by the TEM image (Figure 2E), corresponding to the SEM image. We can find that the color of the products changes from dark black to light gray after etching the Fe_3O_4 cores, and the size and shape of SiO_2 capsules stay unchanged. Close observation reveals that the respective thicknesses of the shell are measured to be around 10, 12, 13, 14, and 16 nm (Figure 3A2, B2, C2, D2, and E2). The mesoporous pores in the shell make the $Gd(NO_3)_3$ ethanol solution diffuse in or out, leading to HMSC@ Gd_2O_3:Yb/Tm, as shown in Figure 3A3, B3, C3, D3, and E3. It can also be seen that the shapes and sizes of all HMSC@ Gd_2O_3:Yb/Tm match well with the SEM images. It is noted that the thickness of the shells is increased slightly compared with pure HMSC due to the deposited Gd_2O_3:Yb/Tm.

dx.doi.org/10.1021/ic501121t | Inorg. Chem. 2014, 53, 10917–10927

Figure 3A exhibits the XRD pattern of as-prepared HMSC-C@Gd_2O_3:Yb/Tm. It is found that the diffraction peaks can be directly indexed to orthorhombic phased Gd_2O_3 (JCPDS No. 86-2477). The broad weak peak at ~22° is associated with the amorphous silica. As studied above, the TEM and SEM images (Figure 3B–D) can clearly confirm the hollow structure of the product. In Figure 3E for the HRTEM image, the clear lattice fringes reveal the crystalline nature of Gd_2O_3. The determined interplanar distance (0.31 nm) corresponds to the d_{111} spacing of orthorhombic phased Gd_2O_3 (JCPDS No. 86-2477), which is also confirmed by the fast Fourier transform (FFT) pattern (inset in panel E), showing the diffraction spots of the (111) planes of orthorhombic Gd_2O_3. From the energy-dispersive spectrometry (EDS) (Figure 3F), we can observe Si, O, and Gd elements and the weak C peak is assigned to the carbon conductive tape. Yb and Tm elements cannot be detected because of the low doping concentration. The calculated mass weight percent of Gd element from the EDS result is 12.7 wt %, which basically agrees with the inductively coupled plasma (ICP) result (13.1 wt %). In addition, from the TEM mapping (Figure 3F), we can see that Gd and Yb atoms uniformly disperse on the surface of hollow silica spheres.

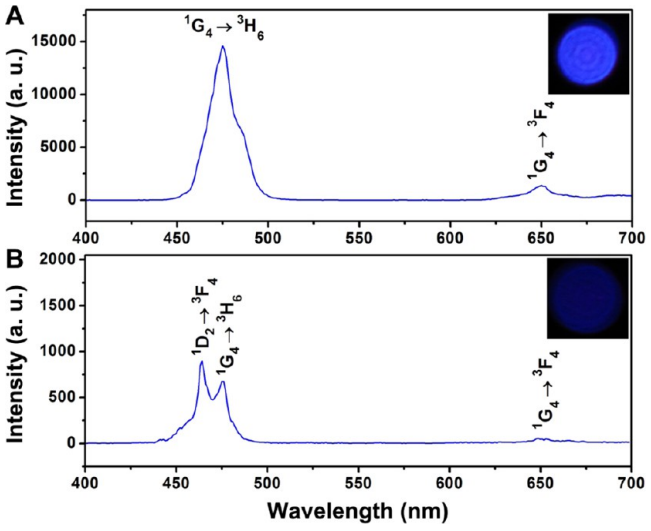

Figure 6. UC emission spectra of HMSC-C@Gd_2O_3:Yb/Tm (A) and HMSC-C@Gd_2O_3:Yb/Tm-DOX (B) under 980 nm laser diode (LD) excitation. Insets are their corresponding luminescent photographs at 980 nm irradiation in the dark.

To ascertain the formation of mesoporous structure, the nitrogen sorption properties of HMSC@Gd_2O_3:Yb/Tm are investigated and depicted in Figure 4. As shown, all adsorption/desorption isotherms (Figure 4, left) belong to the characteristic IV isotherms together with H1 hysteresis loops associated with typical mesoporous materials. The textural parameters of HMSC@Gd_2O_3:Yb/Tm with different particle sizes and shapes are summarized in Table 1. We can see that all the HMSC@Gd_2O_3:Yb/Tm hollow capsules possess high specific surface area and high pore volume. The corresponding surface area and pore volume of HMSC-C@Gd_2O_3:Yb/Tm is 461 m^2/g and 1.51 cm^3/g, respectively, indicating its high potential in drug release. The relatively wide pore size distribution should be due to the unique structure.

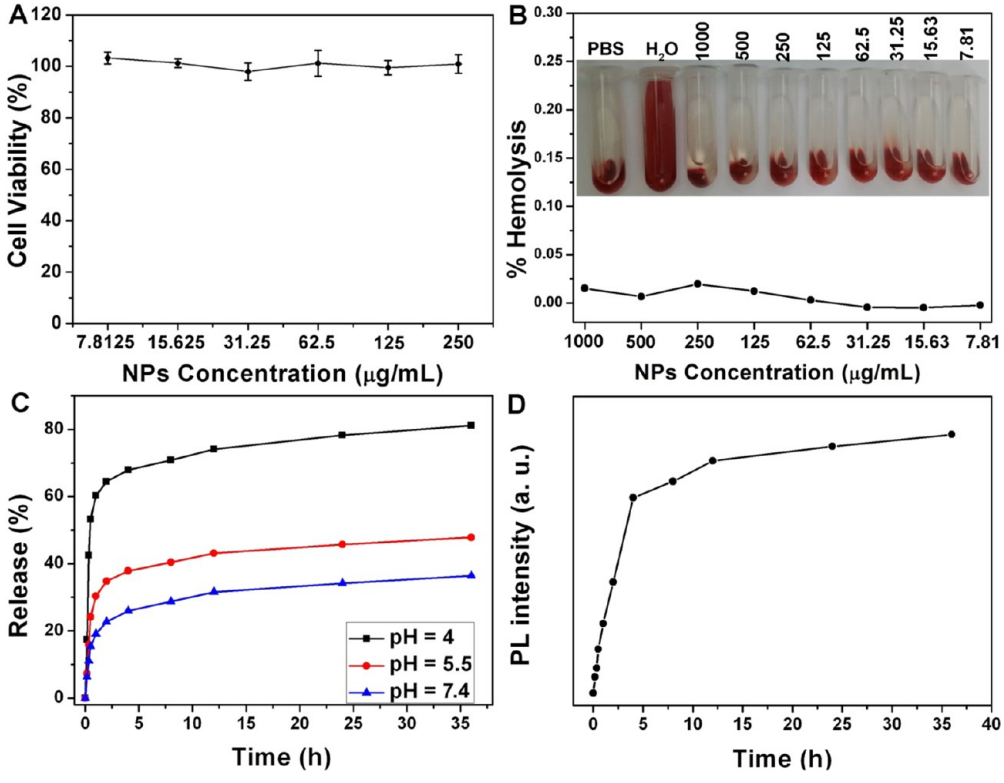

Figure 7. Cell viability of L929 fibroblast cell incubated for 24 h with HMSC-C@Gd_2O_3:Yb/Tm with different concentrations (A), the hemolysis percentage of HMSC-C@Gd_2O_3:Yb/Tm to human red blood (B), the cumulative DOX releases from HMSC-C@Gd_2O_3:Yb/Tm in PBS buffer at pH = 4, 5.5, and 7.4 as a function of the release time (C). UC photoluminescence (PL) emission intensity of Tm^{3+} at pH = 4 as a function of the release time (D).

dx.doi.org/10.1021/ic501121t | Inorg. Chem. 2014, 53, 10917–10927

Figure 5 presents the FT-IR spectra of pure DOX, HMSC-C@Gd_2O_3:Yb/Tm, and HMSC-C@Gd_2O_3:Yb/Tm-DOX, respectively. In Figure 5B for HMSC-C@Gd_2O_3:Yb/Tm, a weak peak at 1623 cm^{-1} and a broad shoulder at 3600−3200 cm^{-1} are assigned to O−H vibration and the OH^- ions of H_2O molecules adsorbed on the outside. The typical vibrations of SiO_2 such as Si−O−Si (1080 cm^{-1}) and Si−OH (988 cm^{-1}) can also be detected. For DOX-carried capsule (Figure 5C), two weak peaks centered at 2933 and 2853 cm^{-1} should be assigned to $-CH_3$ and the asymmetric band of $-CH_2-$, while some sharp peaks at 1457 and 1709 cm^{-1} can be related to the C═O stretching vibration of DOX molecules (Figure 5A) on the carrier surface. This confirms the existence of drug molecules on the carrier surface.

UC Luminescent Properties. Figure 6 depicts the emission spectra of HMSC-C@Gd_2O_3:Yb/Tm and HMSC-C@Gd_2O_3:Yb/Tm-DOX, respectively. It shows that both of the products exhibit the typical emissions of Tm^{3+} under 980 nm NIR excitation except for a change in the emission intensity. In Figure 6A, the dominated blue emission at ∼475 nm can be assigned to $^1G_4 \rightarrow {}^3H_6$ transition, and the peak at 650 nm is attributed to the $^1G_4 \rightarrow {}^3F_4$ electron transition of Tm^{3+} ions.[70,71] From Figure 6B for the DOX-loaded sample, we can see that the dc intensity is markedly decreased. It is known that high-frequency phonon vibrations of the organic group in drug molecules may markedly quench the luminescence.[39] It is noted that the UC emission obviously can still be detected in the DOX-loaded carrier (Figure 6B), making it possible to track and detect the released drug simultaneously.

MTT Assay, Drug Carrying, and Release Properties. To achieve biological application, we used MTT cell assay performed on L929 cell to measure the short-term viability of HMSC-C@Gd_2O_3:Yb/Tm. Figure 7A shows the cell viability with a serious concentration of HMSC-C@Gd_2O_3:Yb/Tm from 7.8125 to 250 μg/mL. It is obvious that the cell viability of the sample in all dosages reaches 99%−105%. Even at high concentration of 250 μg/mL, 102.5% cell viability is still achieved. The results indicate that the cell grows normally under different concentration of the particles, and the higher cell viability (>100%) is a normal state owing to an irregularly rapid cell growth, which has been extensively studied.

Such a low in vitro cytotoxicity proved by MTT assay offers an essential promise for potential in vivo drug carrier. To ensure the successful intravenous administration as the antitumor chemotherapy, it is essential to detect the biocompatibility of the materials with blood cells. Figure 7B shows the hemolytic results. The red blood cells were separated from freshly obtained EDTA.K2, which was stabilized human blood through centrifugation then purification by successive rinsing with 1% normal saline. After adding the materials in the diluted cells for 2 h, the hemolytic activity was measured by UV−vis. The cell solution is red because of the presence of hemoglobin. In the hemolysis assay process, the obtained red solution (dissolved with H_2O) caused by hemolysis is attributed to the hemoglobin released into the solution. For the controlled tubes with the PBS and the materials with different solutions added, there is no visually obvious red that occurred, which indicates there is no or negligible hemolysis. The highest hemolytic efficiency with different material concentrations from 7.81 to 1000 μg/mL is 0.02%, which indicates the HMSC@Gd_2O_3:Yb/Tm is almost not hemolytic. In conclusion, the blood compatibility of the as-synthesized materials is excellent. Combined with the L929 viability test, it is inferred that the sample has high biocompatibility.

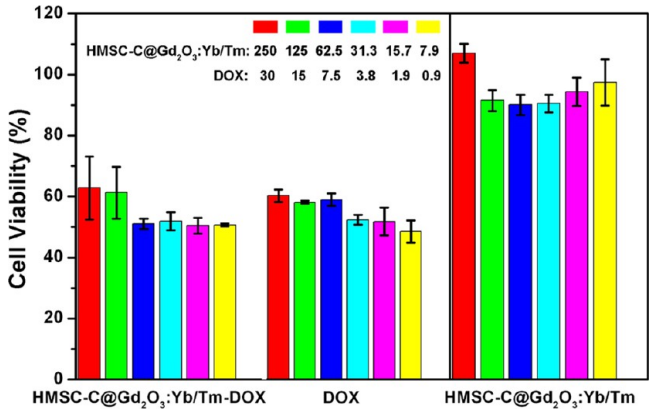

Figure 8. Viabilities of HeLa cells incubated for 24 h with free DOX, HMSC-C@Gd_2O_3:Yb/Tm-DOX, and pure HMSC-C@Gd_2O_3:Yb/Tm with different concentrations.

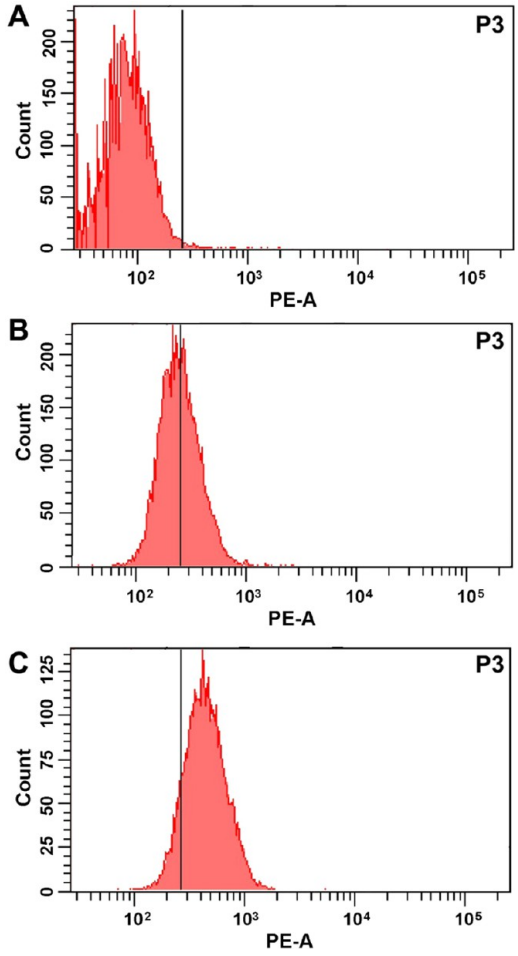

Figure 9. Flow cytometry analysis of the control cells (A) and HeLa cells incubated with HMSC-C@Gd_2O_3:Yb/Tm-FITC composites for 0.5 h (B) and 3 h (C).

DOX was used as a model drug to study the drug-carrying and -release capacity of HMSC-C@Gd_2O_3:Yb/Tm capsules. The respective loading efficiency is 9.1% and 14.4% for the carrier after reacting for 1 and 3.5 h. After stirring for 24 h, 84.4% of the DOX have been loaded by the HMSC-C@Gd_2O_3:Yb/Tm capsules. It should be noted that the loading efficiency of solid silica with a similar particle size (∼220 nm) of HMSC-C@Gd_2O_3:Yb/Tm is only 11.8% after immersing for

dx.doi.org/10.1021/ic501121t | Inorg. Chem. 2014, 53, 10917−10927

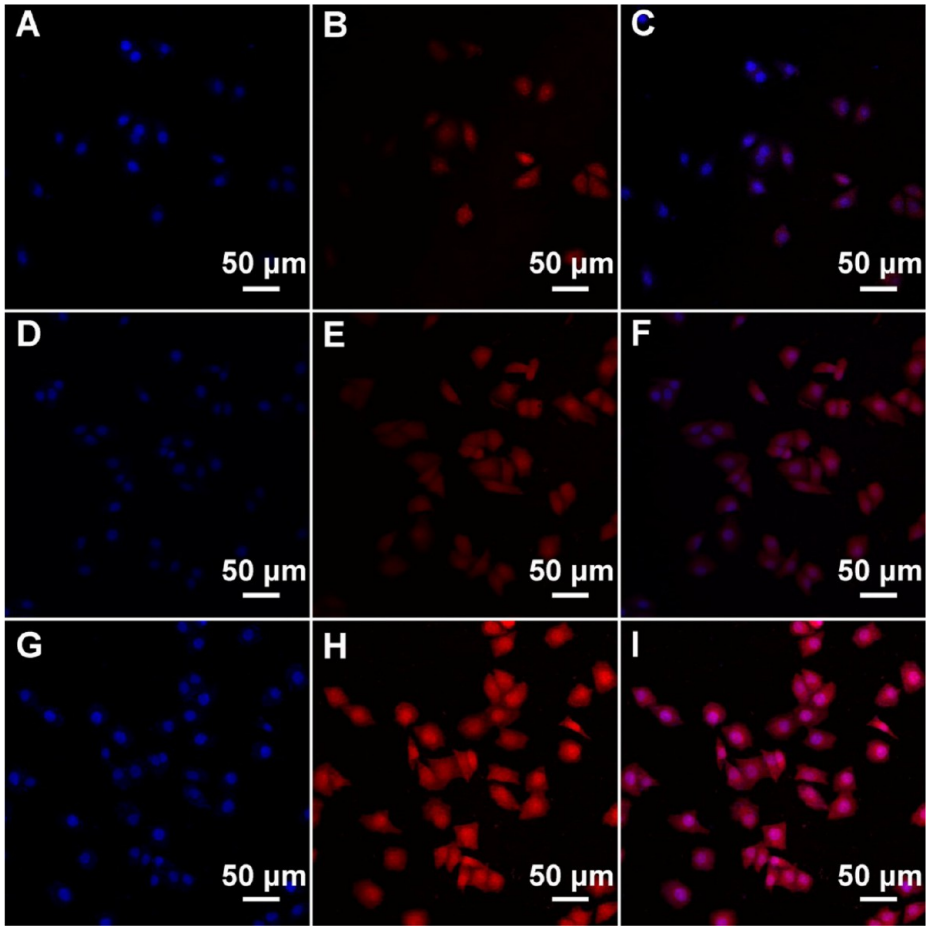

Figure 10. Confocal laser scanning microscope (CLSM) of HMSC-C@Gd_2O_3:Yb/Tm composites cells incubated with HeLa cells for 0.5 h (A–C), 3 h (D–F), and 6 h (G–I).

24 h, which can be ascribed to the low specific surface area (5.1 m^2/g). Hence, the functional capsule that reacted for 24 h was selected to evaluate the in vitro drug-carrying and -release properties. Figure 7C shows the accumulated release profiles of DOX released from HMSC-C@Gd_2O_3:Yb/Tm-DOX in PBS buffer at different conditions (pH = 4, 5.5, and 7.4) at 37 °C. With the decreased pH value, higher release efficiency and rate are obtained due to the increased positive charge of the materials, which promotes the release of positive-charged DOX. In general, many solid tumors have an acidic extracellular circumstance because of the hypoxia-induced coordinated upregulation of glycolysis, which is lower than that of normal tissues. After being engulfed by cells, the particles first come into endosomes, then lysosomes, and finally fuse with lysosomes. Endosomes (pH = 5.0–6.0) and lysosomes (pH = 4.5–5.0) both belong to an acidic environment, which differs from the outside environment (pH = 7.4). Thus, the pH-sensitive bifunctional carrier is promising as a drug carrier and good for the targeting of cancerous tissues. The release efficiencies with the three different conditions have the same tendency with increased time. In the initial 1 h, the release efficiencies are 60.2%, 30.4%, and 19.1% with pH values of 4, 5.5, and 7.4, respectively. After that, there are slow enhanced release efficiencies during the last times. In the end, the efficiencies of the three conditions are 81.2%, 47.8%, and 36.4%, respectively. The initial fast release could kill most of the cancer cells, and the rest of the slow release can ensure the killing of the cancer cells that survived. Figure 7D is the UC emission intensity of Tm^{3+} at pH = 7.4 at different release times. It is apparent that the UC emission intensity is enhanced with the release of DOX, reaching its maximum as the release is complete. The result indicates the promising candidate of this functional carrier to be monitored or detected by the change of UC emission during the release process.

MTT assay was employed to test the pharmacological activity of DOX-loaded HMSC-C@Gd_2O_3:Yb/Tm on human HeLa cells. As an effective, broad-spectrum chemotherapeutic drug, DOX has been widely used as clinical medicine. However, DOX has a toxic influence on normal tissues, such as cardiac toxicity and brain tissue, which is even fatal in some cases. In this research, DOX was loaded on the pH-responsive carriers, which favors it releasing at the target tumor sites and could greatly decrease the toxicity and side effects of DOX. Figure 8 presents the cell viabilities against pure DOX, HMSC-C@Gd_2O_3:Yb/Tm-DOX, and HMSC-C@Gd_2O_3:Yb/Tm at diverse concentrations after incubation for 24 h. It can be seen that the blank HMSC-C@Gd_2O_3:Yb/Tm has no apparent cytotoxic influence on tumor cells even after being treated for 24 h with a high concentration of 250 μg/mL. The concentrations of free DOX were kept to be the same as the DOX released from the DOX-loaded HMSC-C@Gd_2O_3:Yb/Tm system after 24 h. The cell viabilities incubated with free DOX and HMSC-C@Gd_2O_3:Yb/Tm-DOX both decrease with the increase of DOX concentration. At the lower concentration, pure DOX exhibits a trivially higher cytotoxicity than HMSC-C@Gd_2O_3:Yb/Tm-DOX. However, the DOX-carried capsule shows similar cytotoxicity to

dx.doi.org/10.1021/ic501121t | Inorg. Chem. 2014, 53, 10917–10927

that of pure DOX, when the particle concentration is increased to 15.7 μg/mL (DOX concentration = 1.9 μg/mL). This may be because small DOX molecules can rapidly diffuse into cells while the capsule has to be endocytosed to enter the cells. Thus, free DOX is faster than the DOX-carried capsule by cellular uptake. As the amount is further increased, more DOX-carried capsules can be endocytosed to reach the tumor cells and release DOX inside to induce tumor death. At the cellular level, most internalization of particles will take place through endocytosis.

Cellular-Uptake Behavior. Cellular-uptake properties of DOX-carried HMSC-C@Gd_2O_3:Yb/Tm-FITC were investigated by flow cytometry. First, the cell uptake degrees of the capsules were quantified with flow cytometry by measuring the signal of DOX from DOX-loaded HMSC-C@Gd_2O_3:Yb/Tm treated with HeLa cells. In Figure 9, after incubation of HeLa cells with the sample for 30 min and 3 h, the median fluorescence levels in the PE−A histograms show that HMSC-C@Gd_2O_3:Yb^{3+}/Tm^{3+}-DOX capsules were taken up by the cells in comparison with the controlled HeLa cells, and the cell uptake of the capsule gradually increases with the increased time of incubation.

The CLSM images of HeLa cancer cells incubated with as-prepared HMSC-C@Gd_2O_3:Yb/Tm+DOX at 37 °C for 30 min, 3 h, and 6 h were further taken to verify the cell-uptake process. From Figure 10, we can see that each series could be classified into the red emissions of nuclei dyed by DAPI irradiated at 405 nm, the red emissions by DOX irradiated at 543 nm, and an overlay of the two channels, respectively. In the first 30 min, there is little red emission, which indicates only some of the particles were taken up by the cells. When the time of incubation was increased to 3 h, stronger red emissions were detected. The red luminescence of DOX was found in both the cell nucleus and the cytoplasm. Finally, almost all of the composites have passed through the membrane and are localized in the cytoplasm with the increased incubation time of 6 h. On the basis of the time course of the CLSM result, it is inferred that the capsules can be taken up by cancer cells effectively. According to the results, the HMSC-C@Gd_2O_3:Yb/Tm capsules can be potentially employed as a carrier to load and transfer antitumor drugs and improves the efficiency of antitumor drug delivery.

CONCLUSIONS

In summary, a novel kind of SiO_2@Gd_2O_3:Yb/Tm hollow capsule has been successfully prepared via a hard-templating procedure using different sized iron oxides as cores, followed by introduction of a UC emission layer. The obtained hollow structured capsules show blue UC fluorescence under 980 nm NIR laser excitation even after carrying DOX molecules. This functional carrier shows sustained release properties as well as low short-term cytotoxicity to L929 cells. The release of DOX from SiO_2@Gd_2O_3:Yb/Tm-DOX is pH-sensitive. Particularly, the intensity of UC emission for drug-carried carrier increases with the released DOX, offering the possibility to be detected or monitored by the change of the luminescence. Therefore, this kind of functional hollow capsule supplies a platform for biomedical applications in drug delivery.

AUTHOR INFORMATION

Corresponding Author

* E-mail: yangpiaoping@hrbeu.edu.cn.

Notes

The authors declare no competing financial interest.

ACKNOWLEDGMENTS

This work was supported by funding from financial supports from the National Natural Science Foundation of China (NSFC 21271053, 21401032, 51472058), Natural Science Foundation of Heilongjiang Province (LC2012C10), Research Fund for the Doctoral Program of Higher Education of China (20112304110021), Program for New Century Excellent Talents in University, Harbin Sci.-Tech. Innovation Foundation (RC2012XK017012), and the Fundamental Research Funds for the Central Universities of China (HEUCF201403006), which are greatly acknowledged.

REFERENCES

(1) Yang, P. P.; Gai, S. L.; Lin, J. *Chem. Soc. Rev.* **2012**, *41*, 3679−3698.
(2) Liu, Y. S.; Tu, D. T.; Zhu, H. M.; Chen, X. Y. *Chem. Soc. Rev.* **2013**, *42*, 6924−6958.
(3) Zeng, S. J.; Wang, H. B.; Lu, W.; Yi, Z. G.; Rao, L.; Liu, H. R.; Hao, J. H. *Biomaterials* **2014**, *35*, 2934−2941.
(4) Li, X. M.; Zhang, F.; Zhao, D. Y. *Nano Today* **2013**, *8*, 643−676.
(5) Xu, Z. H.; Ma, P. A.; Li, C. X.; Hou, Z. Y.; Zhai, X. F.; Huang, S. S.; Lin, J. *Biomaterials* **2011**, *32*, 4161−4173.
(6) Sharma, A. K.; Son, K. H.; Han, B. Y.; Sohn, K.-S. *Adv. Funct. Mater.* **2010**, *20*, 1750−1755.
(7) Xue, X. J.; Wang, F.; Liu, X. G. *J. Mater. Chem.* **2011**, *21*, 13107−13127.
(8) Wang, L. Y.; Bao, J.; Wang, L.; Zhang, F.; Li, Y. D. *Chem.—Eur. J.* **2006**, *12*, 6341−6347.
(9) Uhrich, K. E.; Cannizzaro, S. M.; Langer, R. S.; Shakesheff, K. M. *Chem. Rev.* **1999**, *99*, 3181−3198.
(10) Nasongkla, N.; Shuai, X.; Ai, H.; Weinberg, B. D.; Pink, J.; Boothman, D. A.; Gao, J. *Angew. Chem., Int. Ed.* **2004**, *43*, 6323−6327.
(11) Zhou, J.; Lu, Z. G.; Zhu, X. J.; Wang, X. J.; Liao, Y.; Ma, Z. F.; Li, F. Y. *Biomaterials* **2013**, *34*, 9584−9592.
(12) Slowing, I. I.; Trewyn, B. G.; Giri, S.; Lin, V. S. Y. *Adv. Funct. Mater.* **2007**, *17*, 1225−1236.
(13) Liu, Y.; Sun, Y.; Cao, C.; Yang, Y.; Wu, Y. Q.; Ju, D. W.; Li, F. Y. *Biomaterials* **2014**, *35*, 3348−3355.
(14) Yang, D.; Kang, X.; Ma, P. A.; Dai, Y.; Hou, Z.; Cheng, Z.; Li, C.; Lin, J. *Biomaterials* **2013**, *34*, 1601−1612.
(15) Chen, Y.; Chen, H.; Guo, L.; He, Q.; Chen, F.; Zhou, J.; Feng, J.; Shi, J. *ACS Nano* **2009**, *4*, 529−539.
(16) Topete, A.; Alatorre-Meda, M.; Lglesias, P.; Villar-Alvarez, E. M.; Barbosa, S.; Costoya, J. A.; Taboada, P.; Mosquera, V. *ACS Nano* **2014**, *8*, 2725−2738.
(17) Zhu, Y.; Shi, J.; Shen, W.; Dong, X.; Feng, J.; Ruan, M.; Li, Y. *Angew. Chem., Int. Ed.* **2005**, *44*, 5083−5087.
(18) Doherty, C. M.; Buso, D.; Hill, A. J.; Furukawa, S.; Kitagawa, S.; Falcaro, P. *Acc. Chem. Res.* **2014**, *47*, 396−405.
(19) Vallet-Regí, M.; Balas, F.; Arcos, D. *Angew. Chem., Int. Ed.* **2007**, *46*, 7548−7558.
(20) Tong, L.; Shi, J.; Liu, D.; Li, Q.; Ren, X.; Yang, H. *J. Phys. Chem. C* **2012**, *116*, 7153−7157.
(21) Zhao, D.; Feng, J.; Huo, Q.; Melosh, N.; Fredrickson, G. H.; Chmelka, B. F.; Stucky, G. D. *Science* **1998**, *279*, 548−552.
(22) Vallet-Regi, M.; Rámila, A.; del Real, R. P.; Pérez-Pariente, J. *Chem. Mater.* **2001**, *13*, 308−311.
(23) Muñoz, B.; Rámila, A.; Pérez-Pariente, J.; Díaz, I.; Vallet-Regí, M. *Chem. Mater.* **2003**, *15*, 500−503.
(24) Lai, C.-Y.; Trewyn, B. G.; Jeftinija, D. M.; Jeftinija, K.; Xu, S.; Jeftinija, S.; Lin, V. S. Y. *J. Am. Chem. Soc.* **2003**, *125*, 4451−4459.
(25) Chen, Y.; Chen, H.; Zeng, D.; Tian, Y.; Chen, F.; Feng, J.; Shi, J. *ACS Nano* **2010**, *4*, 6001−6013.
(26) Deng, Y.; Qi, D.; Deng, C.; Zhang, X.; Zhao, D. *J. Am. Chem. Soc.* **2008**, *130*, 28−29.
(27) Jiao, J.; Jumas, F.-C.; Womes, M.; Chadwick, A. V.; Harrison, A.; Bruce, P. G. *J. Am. Chem. Soc.* **2006**, *128*, 12905−12909.

(28) Zhu, Y.; Ikoma, T.; Hanagata, N.; Kaskel, S. *Small* **2010**, *6*, 471−478.
(29) Sinha, A. K.; Seelan, S.; Tsubota, S.; Haruta, M. *Angew. Chem., Int. Ed.* **2004**, *43*, 1546−1548.
(30) Guerrero-Martínez, A.; Pérez-Juste, J.; Liz-Marzán, L. M. *Adv. Mater.* **2010**, *22*, 1182−1195.
(31) Kim, J.; Kim, H. S.; Lee, N.; Kim, T.; Kim, H.; Yu, T.; Song, I. C.; Moon, W. K.; Hyeon, T. *Angew. Chem., Int. Ed.* **2008**, *47*, 8438−8441.
(32) Kim, J.; Lee, J. E.; Lee, J.; Yu, J. H.; Kim, B. C.; An, K.; Hwang, Y.; Shin, C.-H.; Park, J.-G.; Kim, J.; Hyeon, T. *J. Am. Chem. Soc.* **2006**, *128*, 688−689.
(33) Morelli, C.; Maris, P.; Sisci, D.; Perrotta, E.; Brunelli, E.; Perrotta, I.; Panno, M. L.; Tagarelli, A.; Versace, C.; Casula, M. F.; Testa, F.; Ando, S.; Nagy, J. B.; Pasqua, L. *Nanoscale* **2011**, *3*, 3198−3207.
(34) Sertchook, H.; Elimelech, H.; Makarov, C.; Khalfin, R.; Cohen, Y.; Shuster, M.; Babonneau, F.; Avnir, D. *J. Am. Chem. Soc.* **2007**, *129*, 98−108.
(35) Vivero-Escoto, J. L.; Taylor-Pashow, K. M. L.; Huxford, R. C.; Della Rocca, J.; Okoruwa, C.; An, H.; Lin, W. *Small* **2011**, *7*, 3519−3528.
(36) Yang, Q.; Ma, S.; Li, J.; Xiao, F.; Xiong, H. *Chem. Commun.* **2006**, 2495−2497.
(37) Dai, Y.; Ma, P. A.; Cheng, Z.; Kang, X.; Zhang, X.; Hou, Z.; Li, C.; Yang, D.; Zhai, X.; Lin, J. *ACS Nano* **2012**, *6*, 3327−3338.
(38) Gai, S.; Yang, P.; Li, C.; Wang, W.; Dai, Y.; Niu, N.; Lin, J. *Adv. Funct. Mater.* **2010**, *20*, 1166−1172.
(39) Schrum, K. F.; Lancaster, J. M.; Johnston, S. E.; Gilman, S. D. *Anal. Chem.* **2000**, *72*, 4317−4321.
(40) Brokmann, X.; Hermier, J. P.; Messin, G.; Desbiolles, P.; Bouchaud, J. P.; Dahan, M. *Phys. Rev. Lett.* **2003**, *90*, 120601.
(41) Lin, Y.-S.; Haynes, C. L. *Chem. Mater.* **2009**, *21*, 3979−3986.
(42) Hao, L.-Y.; Zhu, C.-L.; Jiang, W.-Q.; Chen, C.-N.; Hu, Y.; Chen, Z.-Y. *J. Mater. Chem.* **2004**, *14*, 2929−2934.
(43) Wu, H.; Zhang, S.; Zhang, J.; Liu, G.; Shi, J.; Zhang, L.; Cui, X.; Ruan, M.; He, Q.; Bu, W. *Adv. Funct. Mater.* **2011**, *21*, 1850−1862.
(44) Zhang, L.; Wang, L.; Yang, T.; Liu, C.; Wang, C.; Liu, H.; Wang, Y. A.; Su, Z. *Chem.—Eur. J.* **2012**, *18*, 12512−12521.
(45) Wang, F.; Liu, X. *Acc. Chem. Res.* **2014**, *47*, 1378−1385.
(46) Zhang, F.; Braun, G. B.; Pallaoro, A.; Zhang, Y.; Shi, Y.; Cui, D.; Moskovits, M.; Zhao, D.; Stucky, G. D. *Nano Lett.* **2011**, *12*, 61−67.
(47) Liu, D.; Zhao, D.; Shi, F.; Zheng, K.; Qin, W. *Mater. Lett.* **2012**, *85*, 1−3.
(48) Zhang, M.; Shi, S.; Meng, J.; Wang, X.; Fan, H.; Zhu, Y.; Wang, X.; Qian, Y. *J. Phys. Chem. C* **2008**, *112*, 2825−2830.
(49) Salgueiriño-Maceira, V.; Spasova, M.; Farle, M. *Adv. Funct. Mater.* **2005**, *15*, 1036−1040.
(50) Afanasiev, P. *Chem. Mater.* **1999**, *11*, 1999−2007.
(51) Dokoutchaev, A.; James, J. T.; Koene, S. C.; Pathak, S.; Prakash, G. K. S.; Thompson, M. E. *Chem. Mater.* **1999**, *11*, 2389−2399.
(52) Chang, K. W.; Wu, J. J. *Adv. Mater.* **2005**, *17*, 241−245.
(53) Zhai, X. F.; Yu, M.; Cheng, Z. Y.; Hou, Z. Y.; Ma, P. A.; Yang, D. M.; Kang, X. J.; Dai, Y. L.; Wang, D.; Lin, J. *Dalton Trans.* **2011**, *40*, 12818−12825.
(54) Zhang, F.; Shi, Y.; Zhao, Z.; Ma, B.; Wei, L.; Lu, L. *J. Mater. Sci.* **2014**, *49*, 3478−3483.
(55) Hao, J. H.; Zhang, Y.; Wei, X. H. *Angew. Chem., Int. Ed.* **2011**, *50*, 6876−6880.
(56) Yin, Z.; Zhu, Y. S.; Xu, W.; Wang, J.; Xu, S.; Dong, B.; Xu, L.; Zhang, S.; Song, H. W. *Chem. Commun.* **2013**, *49*, 3781−3783.
(57) Liu, Y.; Zhou, S.; Tu, D.; Chen, Z.; Huang, M.; Zhu, H.; Ma, E.; Chen, X. *J. Am. Chem. Soc.* **2012**, *134*, 15083−15090.
(58) Zhuang, J. L.; Yang, X. F.; Fu, J. X.; Liang, C. L.; Wu, M. M.; Wang, J.; Su, Q. *Cryst. Growth Des.* **2013**, *13*, 2292−2297.
(59) Boyer, J.-C.; van Veggel, F. C. J. M. *Nanoscale* **2010**, *2*, 1417−1419.
(60) Jia, G.; Zheng, Y.; Liu, K.; Song, Y.; You, H.; Zhang, H. *J. Phys. Chem. C* **2009**, *113*, 153−158.
(61) Lei, F.; Yan, B.; Chen, H. H.; Zhao, J. T. *Inorg. Chem.* **2009**, *48*, 7576−7584.
(62) Wang, Y. F.; Liu, G. Y.; Sun, L. D.; Xiao, J. W.; Zhou, J. C.; Yan, C. H. *ACS Nano* **2013**, *7*, 7200−7206.
(63) Zhuang, J. L.; Wang, J.; Yang, X. F.; Williams, I. D.; zhang, W.; Zhang, Q. Y.; Feng, Z. M.; Yang, Z. M.; Liang, C. L.; Wu, M. M. *Chem. Mater.* **2009**, *21*, 160−168.
(64) Gai, S. L.; Li, C. X.; Yang, P. P.; Lin, J. *Chem. Rev.* **2014**, *114*, 2343−2389.
(65) Liu, Z.; Pu, F.; Huang, S.; Yuan, Q. H.; Ren, J. S.; Qu, X. G. *Biomaterials* **2013**, *34*, 1712−1721.
(66) Tian, G.; Gu, Z. J.; Liu, X. X.; Zhou, L. J.; Yin, W. Y.; Yan, L.; Jin, S.; Ren, W.; Xing, M.; Li, S. J. *J. Phys. Chem. C* **2011**, *115*, 23790−23796.
(67) Druon, F.; Velazquez, M.; Veber, P.; Janicot, S.; Viraphong, O.; Buse, G.; Ahmed, M. A.; Graf, T.; Rytz, D.; Georges, P. *Opt. Lett.* **2013**, *38*, 4146−4149.
(68) Xuan, S. H.; Wang, Y. J.; Yu, J. C.; Leung, K. C. *Chem. Mater.* **2009**, *21*, 5079−5087.
(69) Stöber, W.; Fink, A.; Bohn, E. *J. Colloid Interface Sci.* **1968**, *26*, 62−69.
(70) Zheng, W.; Zhou, S. Y.; Chen, Z.; Hu, P.; Liu, Y. S.; Tu, D. T.; Zhu, H. M.; Li, R. F.; Huang, M. D.; Chen, X. Y. *Angew. Chem., Int. Ed.* **2013**, *52*, 6671−6676.
(71) Yin, A. X.; Zhang, Y. W.; Sun, L. D.; Yan, C. H. *Nanoscale* **2010**, *2*, 953−959.